RSC Advances

PAPER

View Article Online
View Journal | View Issue

Cite this: *RSC Adv.*, 2026, **16**, 16505

Facilitating the Fe(III)/Fe(II) redox cycle with organic pollutants to enhance the heterogeneous Fenton-like catalytic performance of iron-containing catalysts

Cong Gao, *[a] Houfen Li,[b] Jize Liu,[a] Wenchao Yang,[a] Hong Chen[a] and Jianbo Han[a]

Received 3rd December 2025
Accepted 9th February 2026

DOI: 10.1039/d5ra09339b

rsc.li/rsc-advances

The heterogeneous Fenton-like reaction is a promissing technology for removing organic pollutants in water. The reduction of Fe(III) to Fe(II), as the rate-limiting step for generating ·OH, is crucial in heterogeneous Fenton-like reactions and may be improved using organic pollutants with lower redox potential than that of Fe(III)/Fe(II). In this work, the rapid reduction of Fe(III) to Fe(II) on the MIL-100-Fe catalyst was achieved by degrading methylene blue (MB, $E_0 = 0.01$ V), which has the desired lower redox potential than that of MIL-100-Fe(III)/Fe(II) ($E_0 = 0.76$ V). By contrast, organic pollutants with higher redox potentials than that of MIL-100-Fe, such as phenol ($E_0 = 0.97$ V) and *p*-nitrophenol ($E_0 = 1.23$ V), were incapable of reducing Fe(III) to Fe(II). As a result, the degradation rate constant of MB was one order of magnitude higher than those of phenol and *p*-nitrophenol. Notably, MB could also promote the reduction of Fe(III) to Fe(II) in the presence of phenol or *p*-nitrophenol; thus, the degradation rate constants of phenol and *p*-nitrophenol were significantly enhanced by 50 and 30 times, respectively. The results revealed that organic pollutants with lower redox potential than that of Fe(III)/Fe(II) could facilitate the reduction of Fe(III) to Fe(II), which is beneficial for producing more ·OH, thus improving the heterogeneous Fenton-like catalytic performance.

1. Introduction

The increasing emissions of refractory organic pollutants in water have evoked global concern because they undermine the health of the environment and organisms. Advanced oxidation processes (AOPs) have emerged as promising alternatives for the treatment of wastewater containing refractory organic pollutants because of the generation of highly oxidative hydroxyl radicals (·OH, $E_0 = 2.80$ V).[1] The Fenton-like reaction has been demonstrated to be one of the most efficient and economical AOPs. In the Fenton-like reaction, ·OH is generated from the catalytic decomposition of H_2O_2 by homogeneous iron ions (Fe^{2+}/Fe^{3+}) or heterogeneous iron-containing catalysts. Recently, heterogeneous Fenton-like catalysts have attracted increasing research attention because of their advantages over homogeneous catalysts, such as a wide working pH range, recyclability and no iron sludge production. Nevertheless, these catalysts generally show low catalytic activities.

In heterogeneous Fenton-like reactions, ·OH is generated from the chain reactions that involve the reduction of Fe(III) and oxidation of Fe(II) by H_2O_2. In the overall reactions, the reaction rate is limited by the low reduction rate of Fe(III) to Fe(II) (0.001–0.02 M^{-1} s^{-1}), which is considered to be the rate-limiting step in Fenton-like reactions.[2] Given the above fact, accelerating the reduction of Fe(III) to Fe(II) is crucial for enhancing the catalytic activity of heterogeneous Fenton-like catalysts.[3] In the last decade, studies have found that the reduction of Fe(III) to Fe(II) can be enhanced in electro-Fenton-like systems and UV-Fenton-like systems.[4–7] However, these processes are energy-consuming and require complex and expensive equipment. Recently, a pathway using reducing agents, such as hydroxylamine, protocatechuic acid, ascorbic acid and bacterial cellulose, to facilitate the reduction of Fe(III) to Fe(II) has evoked intense research attention.[8–13] During the reaction, in addition to H_2O_2, Fe(III) reacts with reducing agents to generate Fe(II). As a result, the redox cycle of Fe(III)/Fe(II) is accelerated. Nevertheless, these reducing agents are generally harmful to the environment. Moreover, they compete with organic pollutants for ·OH consumption during the reaction.

Actually, organic pollutants are important reactants. It is speculated that organic pollutants can work as reducing agents to facilitate the reduction of Fe(III) to Fe(II) without the aid of

[a]*Key Laboratory of Coastal Ecology and Environment of State Oceanic Administration, National Marine Environmental Monitoring Center, Dalian 116023, China. E-mail: cgao@nmemc.org.cn; gaocong.200746033@163.com; Tel: +86-411-84783710*

[b]*College of Environment and Ecology, Taiyuan University of Technology, Taiyuan 030024, China*

energy or additional agents. Theoretically, the reduction of Fe(III) to Fe(II) by substances with lower redox potentials than that of Fe(III)/Fe(II) is thermodynamically feasible. Thus, it is speculated that organic pollutants with lower redox potentials than that of Fe(III)/Fe(II) can facilitate the redox cycle of Fe(III)/Fe(II), as described in eqn (1)–(3). As a result, the Fenton-like catalytic performance can be improved.

$$\equiv Fe^{III} + e^- \rightarrow \equiv Fe^{II}\ E_{Fe(III)/Fe(II)} \quad (1)$$

$$Pollutant^+ + e^- \rightarrow pollutant\ E_{pollutant/pollutant^+} < E_{Fe(III)/Fe(II)} \quad (2)$$

$$Pollutant + \equiv Fe^{III} \rightarrow \equiv Fe^{II} + pollutant^+ \quad (3)$$

In this work, we attempted to explore a method using an organic pollutant to accelerate the redox cycle of Fe(III)/Fe(II) for enhancing the heterogeneous Fenton-like catalytic performance. Iron-based metal–organic frameworks (MOFs) and their related composites have demonstrated superior catalytic performance in AOPs to traditional iron-based catalysts (such as Fe_3O_4 and FeOOH).[14–17] This significant advantage is mainly attributed to their tunable structural properties, abundant active sites and efficient electron transfer capability. Among the diverse family of iron-based MOFs, MIL-100-Fe stands out as an attractive AOP catalyst because of its high surface area (above 1000 $m^2\ g^{-1}$), porous structure and high distribution of trivalent-state Fe(III) sites.[18–20] Moreover, MIL-100-Fe exhibits good reusability and stability, which ensures its long-term catalytic activity in AOPs.[15,21] Consequently, MIL-100-Fe was selected as an ideal catalyst candidate in the present study. Methylene blue (MB, $E_0 = 0.01$ V),[22] which has a lower redox potential than that of Fe(III)/Fe(II) ($E_0 = 0.77$ V), was selected as the organic pollutant. For comparison, phenol ($E_0 = 0.97$ V) and *p*-nitrophenol ($E_0 = 1.23$ V),[23] which have higher redox potentials than that of Fe(III)/Fe(II) ($E_0 = 0.77$ V), were also used as organic pollutants. The relationship between the Fenton-like catalytic performance and the redox potentials of organic pollutants (MB, phenol and *p*-nitrophenol) was investigated in the MIL-100-Fe/H_2O_2 system. Moreover, the degradation of phenol and *p*-nitrophenol in the presence of MB was studied. Finally, a mechanism for the organic pollutant-enhanced heterogeneous Fenton-like catalysis by facilitating the reduction of Fe(III) to Fe(II) was proposed.

2. Experimental

2.1 Chemicals and materials

A zero-valent iron powder, phenol and *p*-nitrophenol were obtained from Bodi Chemical Co., Ltd (Tianjin, China). BTC was supplied by Energy Chemical Corporation (China). Methylene blue (MB), hydrofluoric acid (HF), nitric acid (HNO_3), sodium hydroxide (NaOH), sulfuric acid (H_2SO_4), hydrochloric acid (HCl), 30% (w/w) H_2O_2, sodium thiosulfate ($Na_2S_2O_3$), ethanol and absolute ethyl alcohol were purchased from Damao Chemical Reagent Factory (Tianjin, China) and Fuyu Chemical Co., Ltd (Tianjin, China). A-FeOOH, Fe_2O_3, coumarin and 5,5-dimethyl-1-pyrroline *N*-oxide (DMPO) were obtained from Aladdin Industrial Corporation (China). All chemicals and materials were used without any purification. Ultrapure water (18.2 MΩ cm) was used in the experiments.

2.2 Preparation of MIL-100-Fe

MIL-100-Fe was prepared by a hydrothermal method.[10] The zero-valent iron powder (0.8 g) and BTC (2.0 g) were added to 71.2 mL of ultrapure water containing 1.28 mL of HF and 0.59 mL of HNO_3. The resulting solution was transferred to a 100 mL Teflon-lined stainless-steel autoclave and heated at 170 °C for 12 h. After cooling to room temperature, the obtained solid was rinsed with ultrapure water and absolute ethyl alcohol at 60 °C until the supernatant became colorless. Consequently, the solid was separated and vacuum-dried at 110 °C overnight.

2.3 Characterization of MIL-100-Fe

The X-ray diffraction (XRD) pattern was obtained on an Empyrean diffractometer with Cu Kα radiation (PANalytical, Holland). Attenuated total reflectance Fourier transform infrared (ATR-FTIR) spectroscopy was performed on a 6700 FTIR spectrometer (Thermo Fisher, USA). The morphology of the catalyst was analysed using a Hitachi S-4800 scanning electron microscope (SEM, Japan) and a Tecnai G2 F30 S-Twin type transmission electron microscope (TEM, FEI Company, USA). The specific surface area of the catalyst was determined by N_2 adsorption/desorption experiments using an Autosorb-iQ-C analyzer (Quantachrome, USA). The concentration of dissolved iron ions from the catalyst and the iron content of the catalysts were measured using an Optima 2000DV inductively coupled plasma optical emission spectrometer (ICP, PerkinElmer, USA). The surface species and the oxidation states of iron were determined using an ESCALAB 250XI X-ray photoelectron spectrometer (XPS, Thermo Fisher, USA). The pH_{pzc} (pH at which the surface has no charge) of the catalyst was determined using a Zetasizer nano ZSP (Malvern nano-ZS90, UK).[24] The redox potential of MIL-100-Fe was obtained by linear sweep voltammetry (LSV). The experimental details of pH_{pzc} and LSV measurements are provided in the SI.

2.4 Degradation of organic pollutants on MIL-100-Fe

Three organic pollutants (MB, *p*-nitrophenol and phenol) with different redox potentials were selected. The catalytic degradation experiments were carried out in a 250 mL flask. The initial solution pH was adjusted by sulfuric acid (0.1 M) or sodium hydroxide (0.1 M). MIL-100-Fe (0.1 g L^{-1}) was dispersed in 100 mL of a solution of organic pollutants (100 mg L^{-1}). The mixture was magnetically stirred for 30 min to achieve the adsorption–desorption equilibrium. The reaction was triggered by adding H_2O_2 to the above dispersions under magnetic stirring conditions. At given time intervals, samples were withdrawn, and 1 M $Na_2S_2O_3$ was immediately added to quench the residual reactive oxidative species. Then, the samples were filtered through a 0.22 μm membrane filter, and the concentration of organic pollutants in the filtrate was analyzed.

To investigate the stability and reusability of MIL-100-Fe, the degradation experiment was performed for five cycles. After the

reaction, the catalyst was collected by filtration (through a 0.22 μm filter membrane), washed with ethanol (0.1% HCl), dried in an oven, and used in the next cycle of degradation.

2.5 Analytical methods

The concentration of MB was analyzed using a UV2300 spectrophotometer at $\lambda_{max} = 662$ nm. The concentrations of phenol and *p*-nitrophenol were analyzed *via* high-performance liquid chromatography (HPLC) using an Agilent 1200 HPLC equipped with a C18 reversed-phase column and a Waters 2996 UV detector. The total organic carbon (TOC) values of the samples were determined using a Multi N/C 2100S TOC analyzer (Analytik Jena, Germany). The generated reactive oxidative species (ROS) were detected by electron paramagnetic resonance (EPR) spectroscopy with DMPO as a spin trap and the fluorescence (FL) technique with coumarin as the detection substance.[25] The concentration of dissolved iron ions in the solution was analyzed by inductively coupled plasma optical emission spectroscopy (ICP, PerkinElmer Optima 2000, USA).

3. Results and discussion

3.1 Characterization of MIL-100-Fe

The XRD pattern of the synthesized MIL-100-Fe is illustrated in Fig. S1. The pattern of the synthesized MIL-100-Fe was found to be in accordance with the simulated diffraction pattern, suggesting the successful synthesis of MIL-100-Fe.[10] The BET surface area of the synthesized MIL-100-Fe was measured to be 1379 $m^2\ g^{-1}$. The nitrogen adsorption–desorption isotherm of the synthesized MIL-100-Fe was type I, according to the Brunauer-Deming-Deming-Teller (BDDT) classification (Fig. S2A), which was typical for microporous materials. This result was coincident with the pore size distribution result illustrated in Fig. S2B. The pore size distribution curve exhibited two sharp peaks centered at values of 1.0 nm and 1.4 nm, respectively. As shown in the SEM and TEM pictures (Fig. S3), MIL-100-Fe exhibited an octahedral morphology with a particle size of 1–2 μm.

The zeta potential of MIL-100-Fe at pH 1.0–10.0 is illustrated in Fig. 1A. The pH_{pzc}, at which the zeta potential of MIL-100-Fe was zero, was determined to be 1.2. This suggested that the surface of MIL-100-Fe was positively charged at solution pH < 1.2, whereas the surface was negatively charged at solution pH > 1.2. The actual redox potential of MIL-100-Fe(III)/Fe(II) in this work might be different from the standard redox potential of Fe(III)/Fe(II) ($E_0 = 0.77$ V). The actual redox potential of MIL-100-Fe(III)/Fe(II) was obtained by LSV measurements, as shown in Fig. 1B. A peak was observed at 0.33 V, which was attributed to the reduction of Fe(III) to Fe(II). This indicated that the reduction of MIL-100-Fe(III) to MIL-100-Fe(II) could take place at electrode potentials lower than 0.33 V. Therefore, the actual redox potential of MIL-100-Fe(III)/Fe(II) was considered to be 0.33 V. According to eqn (4), the E_0 of MIL-100-Fe(III)/Fe(II) was 0.76 V.

$$E^0 = E + \text{pH} \times 0.059 + 0.197 \quad (4)$$

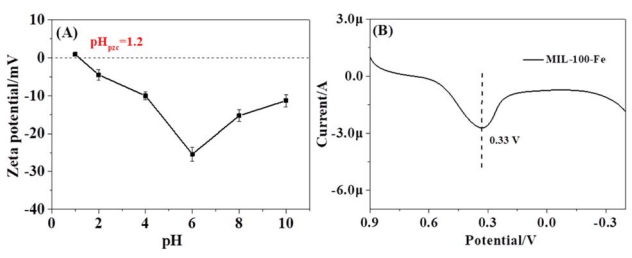

Fig. 1 (A) Zeta potentials of MIL-100-Fe at different values of pH and (B) LSV curve of MIL-100-Fe in the N_2-saturated 0.1 M Na_2SO_4 electrolyte at room temperature.

3.2 Degradation of organic pollutants in the MIL-100-Fe/H_2O_2 system

The degradation of organic pollutants with lower redox potentials (MB, $E_0 = 0.01$ V) and higher redox potentials (phenol, $E_0 = 0.97$ V and *p*-nitrophenol, $E_0 = 1.23$ V) than that of MIL-100-Fe(III)/Fe(II) ($E_0 = 0.76$ V) was conducted at pH 4.0. As shown in Fig. 2A, 5% of phenol and 4% of *p*-nitrophenol were removed in the MIL-100-Fe/H_2O_2 system within 180 min, whereas 83% of MB was removed under the same conditions. The high MB degradation activity of the heterogeneous Fenton-like reaction was further confirmed by the adsorption of MB on MIL-100-Fe and the oxidation of MB by H_2O_2 alone (Fig. 2B), which exhibited MB removal efficiencies of only 28% and 4%, respectively. During the degradation of MB (after achieving the adsorption–desorption equilibrium of MB on MIL-100-Fe), the MB concentration increased from 72 mg L^{-1} to 84 mg L^{-1} in the first 10 min, which might be caused by the desorption of MB from the surface of MIL-100-Fe. At a pH of 4, MB ($pK_a \approx 12.0$) and H_2O_2 ($pK_a = 11.7$) were positively charged, while the surface of MIL-100-Fe was negatively charged. The competitive adsorption of H_2O_2 and MB on the surface of MIL-100-Fe occurred after adding H_2O_2, resulting in an increased MB concentration in the solution. After the reaction for 180 min, the concentration of MB gradually decreased to 17 mg L^{-1}, which could be attributed to the generation of reactive oxidative species (ROS).

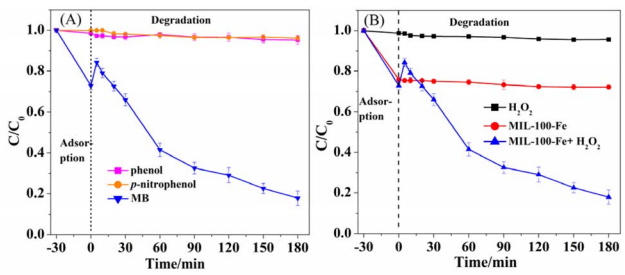

Fig. 2 (A) Degradation of MB, phenol and *p*-nitrophenol in the MIL-100-Fe/H_2O_2 Fenton-like system and (B) degradation of MB by H_2O_2 and the adsorption of MB on MIL-100-Fe. Reaction conditions: [catalyst] = 0.1 g L^{-1}, [H_2O_2] = 16 mM, [organic pollutants] = 100 mg L^{-1}, and pH 4.0 at room temperature.

Table 1 Rate constant and TOC removal efficiency of MB, phenol and *p*-nitrophenol in the MIL-100-Fe/H_2O_2 system. Reaction conditions: [catalyst] = 0.1 g L^{-1}, [H_2O_2] = 16 mM, [organic pollutants] = 100 mg L^{-1}, and pH 4.0 at room temperature

				MB + phenol		MB + *p*-nitrophenol	
Pollutants	MB	Phenol	*p*-Nitrophenol	MB	Phenol	MB	*p*-Nitrophenol
k (min^{-1})	0.9×10^{-2}	0.1×10^{-3}	0.1×10^{-3}	0.6×10^{-2}	0.5×10^{-2}	0.5×10^{-2}	0.3×10^{-2}
TOC (%)	49%	3%	4%	28%		27%	

The degradation of MB, phenol and *p*-nitrophenol could be fitted with pseudo-first-order kinetics. As shown in Table 1, the degradation rate constants of MB, phenol and *p*-nitrophenol were 0.9×10^{-2} min^{-1}, 0.1×10^{-3} min^{-1}, and 0.1×10^{-3} min^{-1}, respectively. The degradation rate constant of MB was one order of magnitude higher than those of phenol and *p*-nitrophenol. Actually, the removal of organic pollutants does not mean their complete degradation. The TOC analysis was performed to evaluate the mineralization of organic pollutants. Within 180 min, the TOC removal efficiency of MB was 49%, which was much higher than those of the other two organic pollutants. To evaluate the catalytic performance of MIL-100-Fe, the TOC removal efficiency of MB was compared with that of representative Fenton-like catalysts reported in the literature. As shown in Table S1, the specific TOC removal efficiency for the dye per unit mass of the catalyst in this study was higher than that of other heterogeneous Fenton-like catalysts reported in previous works, highlighting the excellent Fenton-like catalytic performance of the MIL-100-Fe in dye degradation.

Moreover, the concentration of leached iron ions from MIL-100-Fe during the reaction (Fig. S5) and the Fenton-like catalytic performance of the leached iron were investigated. It can be seen that the concentration of leached iron gradually increased to 0.13 mg L^{-1} within 180 min, which corresponded to 0.5% of the added Fe in MIL-100-Fe. The degradation of MB by leached iron ions (0.13 mg L^{-1}) was investigated. As shown in Fig. S6, only 3% of MB was degraded in the homogeneous Fenton-like reaction within 180 min. Thus, the homogeneous Fenton-like catalysis induced by the leached iron ions was limited. The degradation of MB was dominated by heterogeneous catalysis by MIL-100-Fe.

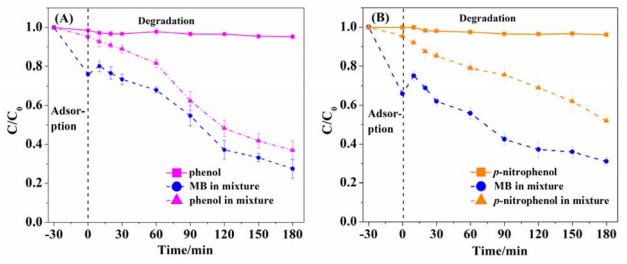

Fig. 3 (A) Degradation of phenol and a mixture of phenol and MB and (B) degradation of *p*-nitrophenol and a mixture of *p*-nitrophenol and MB in the MIL-100-Fe/H_2O_2 Fenton-like system. Reaction conditions: [catalyst] = 0.1 g L^{-1}, [H_2O_2] = 16 mM, [organic pollutants] = 100 mg L^{-1}, and pH 4.0 at room temperature.

The different catalytic performances of MIL-100-Fe toward MB, phenol and *p*-nitrophenol might be attributed to their different redox potentials. Thermodynamically, a substance with a lower redox potential could reduce a substance with a higher redox potential. It was speculated that MB (E_0 = 0.01 V) with a redox potential lower than that of MIL-100-Fe(III)/Fe(II) (E_0 = 0.76 V) could facilitate the reduction of Fe(III) to Fe(II) in MIL-100-Fe, thus producing more $^{\cdot}OH$ for pollutant degradation in the Fenton-like reaction. In order to verify that MB could enhance the Fenton-like catalytic performance, the degradation of phenol and *p*-nitrophenol in the presence of MB was investigated in the MIL-100-Fe/H_2O_2 system. As shown in Fig. 3A, when phenol and MB were mixed together, 72% of MB and 63% of phenol were degraded in the MIL-100-Fe-catalyzed Fenton-like system within 180 min. As illustrated in Table 1, the degradation rate constant of phenol in the presence of MB was one order of magnitude higher than that in the absence of MB. The degradation rate constant of MB was slightly lower in the mixed organic pollutant solution, which was probably due to the competition for hydroxyl radicals in the mixture. A similar phenomenon was also observed during the degradation of *p*-nitrophenol in the presence of MB (Fig. 3B). In the mixture of *p*-nitrophenol and MB, the degradation efficiencies of MB and *p*-nitrophenol were 69% and 49%, respectively. The degradation rate constant of *p*-nitrophenol improved by one order of magnitude in the presence of MB. The above results demonstrated that MB could enhance the heterogeneous Fenton-like catalytic efficiency for degrading organic pollutants. To further verify this finding, the performance of the MIL-100-Fe-catalyzed heterogeneous Fenton-like system in the absence and presence of MB during real wastewater treatment was further evaluated using actual dyeing wastewater that had undergone secondary biological treatment, followed by activated carbon adsorption. The initial TOC concentration of the dyeing wastewater was determined to be 40.1 mg L^{-1}. As shown in Fig. S7, the TOC removal efficiency of the dyeing wastewater by the MIL-100-Fe-catalyzed Fenton-like reaction was 11.3% after 180 min. In contrast, in the presence of MB, the TOC removal efficiency significantly increased to 20.3%. These results reaffirmed that MB could enhance the performance of the MIL-100-Fe-catalyzed Fenton-like system.

To investigate the reproducibility of this process, the degradation of both MB and phenol by the reused MIL-100-Fe-catalyzed Fenton-like system was analyzed over five consecutive cycles. As illustrated in Fig. 4A, the degradation efficiency of phenol in the presence of MB remained almost unchanged, further confirming that MB could enhance the Fenton-like

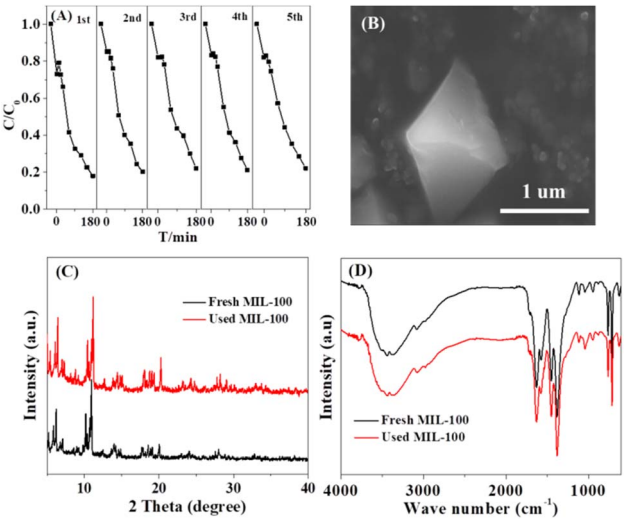

Fig. 4 (A) Degradation of both phenol and MB by the reused MIL-100-Fe in the Fenton-like reaction; (B) SEM image of MIL-100-Fe after the reaction; (C) XRD pattern of MIL-100-Fe after the reaction; and (D) IR spectrum of MIL-100-Fe after the reaction. Reaction conditions: [catalyst] = 0.1 g L^{-1}, [H_2O_2] = 16 mM, [MB] = 100 mg L^{-1}, [phenol] = 100 mg L^{-1}, and pH 4.0 at room temperature.

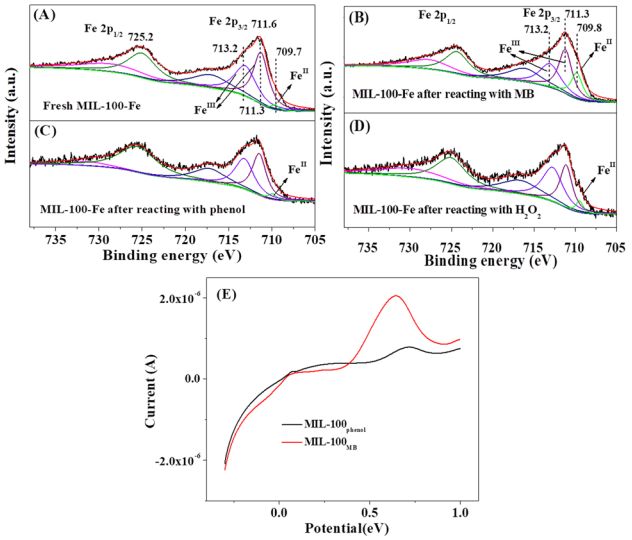

Fig. 5 (A) Fe 2p XPS spectra of fresh MIL-100-Fe; (B) Fe 2p XPS spectra of MIL-100-Fe after reacting with MB for 30 min (MIL-100-Fe_{MB}); (C) Fe 2p XPS spectra of MIL-100-Fe after reacting with phenol for 30 min (MIL-100-Fe_{phenol}); and (D) Fe 2p XPS spectra of MIL-100-Fe after reacting with H_2O_2 for 30 min (MIL-100-$Fe_{H_2O_2}$). (E) LSV curves of MIL-100-Fe_{MB} and MIL-100-Fe_{phenol}. Reaction conditions: [catalyst] = 0.1 g L^{-1}, [H_2O_2] = 16 mM, [MB] = 100 mg L^{-1}, [phenol] = 100 mg L^{-1}, and pH 4.0 at room temperature.

catalytic performance of MIL-100-Fe, and MIL-100-Fe could be reused for at least five cycles. Moreover, the used MIL-100-Fe after five cycles was characterized by SEM, XRD, and IR analyses (Fig. 4B–D, respectively). No obvious changes in the morphology, crystal phase or structure were observed after the reaction, suggesting that MIL-100(Fe) exhibited good stability under the applied catalytic conditions.

3.3 Reaction mechanism

The enhanced heterogeneous Fenton-like catalytic performance of MIL-100-Fe for degrading other organic pollutants by MB might be caused by the accelerated reduction of Fe(III) to Fe(II). To confirm that MB could accelerate the reduction of Fe(III) to Fe(II) in MIL-100-Fe, the chemical states of fresh MIL-100-Fe, MIL-100-Fe after reacting with MB for 30 min (MIL-100-Fe_{MB}) and MIL-100-Fe after reacting with H_2O_2 for 30 min (MIL-100-$Fe_{H_2O_2}$) were analyzed. As shown in Fig. 5A–D, it was obviously observed that the peaks of Fe 2p for MIL-100-Fe shifted to lower binding energies (from 711.6 eV to 711.2 eV and from 725.2 eV to 724.4 eV) after reacting with MB. The deconvolution of the Fe $2p_{3/2}$ peak of MIL-100-Fe_{MB} showed that the ratio of Fe(II) was 21%, which was much higher than that in the fresh MIL-100-Fe (2%, Fig. 5A) and MIL-100-Fe treated with H_2O_2 only (11%, Fig. 5D). This result indicated that MB could facilitate the reduction of Fe(III) to Fe(II) in the MIL-100-Fe/H_2O_2 system.

For comparison, the chemical state of MIL-100-Fe after reacting with phenol (MIL-100-Fe_{phenol}), which has a higher redox potential (E = 1.02 V) than that of MIL-100-Fe(III)/Fe(II) (E = 0.33 V), was analyzed. As shown in Fig. 5C, about 4% of Fe(II) was found on MIL-100-Fe_{phenol}, which was similar to that for the fresh MIL-100-Fe. This suggested that Fe(III) could scarcely be reduced to Fe(II) by phenol on MIL-100-Fe. Further evidence based on the results of LSV is provided in Fig. 5E. The oxidation peak at around 0.65 V was attributed to the oxidation of Fe(II) to Fe(III). It was observed that the oxidation peak of MIL-100-Fe_{MB} was much higher than that of the MIL-100-Fe_{phenol}, indicating that more Fe(II) was generated on MIL-100-Fe_{MB} than on the MIL-100-Fe_{phenol}. The above results confirmed that MB, which has a lower redox potential than that of MIL-100-Fe(III)/Fe(II), could effectively reduce Fe(III) to Fe(II) on MIL-100-Fe.

As is generally accepted, facilitating the reduction of Fe(III) to Fe(II) on catalysts could enhance the generation of ˙OH. The generation of ˙OH was investigated *via* the EPR technique using DMPO as the radical spin-trapping agent. As shown in Fig. 6A, the four-fold peaks with an intensity ratio of 1 : 2 : 2 : 1, attributed to the DMPO-˙OH adducts, were observed in MIL-100-Fe/H_2O_2 and MIL-100-Fe_{MB}/H_2O_2 systems. The intensity of DMPO-˙OH generated in the MIL-100-Fe_{MB}-catalyzed Fenton-like

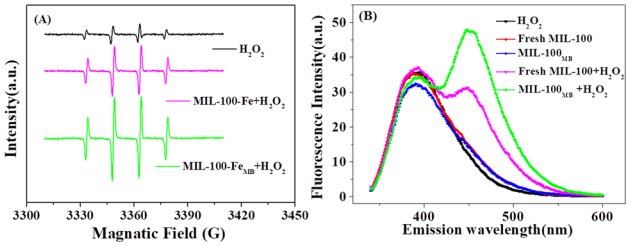

Fig. 6 (A) DMPO-trapped EPR spectra of the MIL-100-Fe/H_2O_2 and MIL-100-Fe_{MB}/H_2O_2 Fenton-like systems and (B) FL spectra of coumarin generated in various reactions. Reaction conditions: [catalyst] = 0.1 g L^{-1}, [H_2O_2] = 16 mM, and pH 4.0 at room temperature.

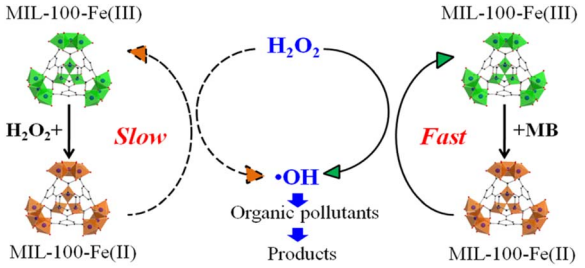

Fig. 7 Reaction mechanism for the enhanced catalytic performance of MIL-100-Fe by MB.

reaction was higher than that in the MIL-100-Fe-catalyzed Fenton-like reaction. Generally, the intensity of the DMPO-•OH peak is positively correlated to the concentration of •OH. Thus, more •OH was produced in the MIL-100-Fe_{MB}-catalyzed Fenton-like reaction than that in the MIL-100-Fe-catalyzed Fenton-like reaction. Moreover, the FL technique using coumarin as the •OH detector substance was employed for the semi-quantitative analysis of the •OH generated in MIL-100-Fe/H_2O_2 and MIL-100-Fe_{MB}/H_2O_2 systems. The PL spectral intensity at about 450 nm (the product of the reaction between •OH and coumarin) is dependent on the amount of •OH generated during the reaction.[26] As shown in Fig. 6B, a higher FL spectral intensity at about 450 nm was observed in the MIL-100-Fe_{MB}-catalyzed Fenton-like reaction than that in the MIL-100-Fe-catalyzed Fenton-like reaction, further indicating that more •OH was generated in the MIL-100-Fe_{MB}-catalyzed Fenton-like reaction.[27]

On the basis of the above results, a possible reaction mechanism for the enhanced catalytic performance of MIL-100-Fe by MB was proposed, as shown in Fig. 7. During the reaction, MIL-100-Fe(III) was reduced by MB and H_2O_2 to generate MIL-100-Fe(II). Next, the generated MIL-100-Fe(II) catalyzed the decomposition of H_2O_2, resulting in the generation of •OH and MIL-100-Fe(III). Then, MIL-100-Fe(III) was continuously reduced to MIL-100-Fe(II) by MB and H_2O_2. These reactions formed a cycle that sustained the generation of •OH. Eventually, organic pollutants were degraded by •OH.

4. Conclusions

In summary, MB with a lower redox potential than that of MIL-100-Fe(III)/Fe(II) could reduce MIL-100-Fe(III) to MIL-100-Fe(II), thus accelerating the redox cycle of Fe(III)/Fe(II) and enhancing the heterogeneous Fenton-like catalytic performance for degrading organic pollutants. In the presence of MB, the degradation rate constants of phenol and *p*-nitrophenol were one order of magnitude higher than those in the absence of MB. This work casts a new light on the effect of organic pollutants on the heterogeneous Fenton-like catalytic performance and provides a new strategy to accelerate the redox cycle of Fe(III)/Fe(II) for enhancing the heterogeneous Fenton-like catalytic performance.

Author contributions

Cong Gao: writing – original draft, investigation, methodology, formal analysis, data curation, and funding acquisition. Houfen Li: methodology and formal analysis. Jize Liu: investigation. Wenchao Yang: data curation. Hong Chen: supervision. Jianbo Han: writing – review and editing and resources.

Conflicts of interest

The authors declare that they have no known competing financial interests or personal relationships that could have appeared to influence the work reported in this paper.

Data availability

The data are available from the corresponding author upon reasonable request.

Supplementary information (SI) is available. See DOI: https://doi.org/10.1039/d5ra09339b.

Acknowledgements

This work was supported financially by the National Natural Science Foundation of China (grant number 22306038) and the Doctoral Research Project of National Marine Environment Monitoring Center (grant number 2022-Z-303).

References

1 R. ndreozzi, V. Caprio, A. Insola and R. Marotta, Advanced oxidation processes (AOP) for water purification and recovery, *Catal. Today*, 1999, **53**(1), 51–59.
2 S. Lin and M. D. Gurol, Catalytic decomposition of hydrogen peroxide on iron oxide: kinetics, mechanism, and implications, *Environ. Sci. Technol.*, 1998, **32**(10), 1417–1423.
3 B. Li, L. Zhao, Y. Zhong, L. Zhang, M. Cao, H. Xu and C. Yue, Interface-engineered Fe_3O_4/hydrophilic graphene as recyclable heterogeneous Fenton catalyst for dye degradation enhancement, *Surf. Interf.*, 2026, **80**, 108401.
4 M. Noorjahan, V. D. Kumari, M. Subrahmanyam and L. Panda, Immobilized Fe(III;)-HY: an efficient and stable photo-Fenton catalyst, *Appl. Catal., B*, 2005, **57**, 291–298.
5 T. M. El-Morsi, M. M. Emara, M. H. Hassan, A. E. Bary, A. S. Abd-El-Aziz and K. J. Friesen, Homogeneous degradation of 1,2,9,10-tetrachlorodecane in aqueous solutions using hydrogen peroxide, iron and UV light, *Chemosphere*, 2002, **47**, 343–348.
6 M. Zhou, Q. an, Q. Wang, Y. Jiao, N. Oturan and M. A. Oturan, Degradation of organics in reverse osmosis concentrate by electron-Fenton process, *J. Hazard. Mater.*, 2012, **215–216**, 287–293.
7 J. Xue, M. Yuan, J. Gao, Z. Zhang, M. Wang and S. Ma, Photo-Fenton catalyst Fe(III)@PCN-222 grafted on PVDF membrane for multitasking applications: Oil/water separation, aromatic pollutants degradation and bacterial inactivation, *Process Safety & Environmental Protection*,

Transactions of the Institution of Chemical Engineers Part B, 2023, p. 169.
8 L. Chen, J. Ma, X. Li, J. Zhang, J. Fang, Y. Guan and P. Xie, Strong enhancement on Fenton oxidation by addition of hydroxylamine to accelerate the ferric and ferrous iron cycles, *Environ. Sci. Technol.*, 2011, **45**, 3925–3930.
9 X. Hou, X. Huang, F. Jia, Z. Ai, J. Zhao and L. Zhang, Hydroxylamine promoted goethite surface Fenton degradation of organic pollutants, *Environ. Sci. Technol.*, 2017, **51**, 5118–5126.
10 Y. Qin, F. Song, Z. Ai, P. Zhang and L. Zhang, Protocatechuic acid promoted alachlor degradation in Fe(III)/H_2O_2 Fenton system, *Environ. Sci. Technol.*, 2015, **49**, 7948–7956.
11 S. Meng, P. Zhou, Y. Sun, P. Zhang, C. Zhou, Z. Xiong, H. Zhang, J. Liang and B. Lai, Reducing agents enhanced Fenton-like oxidation (Fe(III)/Peroxydisulfate): Substrate specific reactivity of reactive oxygen species, *Water Res.*, 2022, **218**, 118412.
12 H. Sun, G. Xie, D. He and L. Zhang, Ascorbic acid promoted magnetite Fenton degradation of alachlor: Mechanistic insights and kinetic modelling, *App. Catal. B: Environ.*, 2020, **267**, 118383.
13 F. Liu, J. You, Q. Gao, M. Hu, R. Li, L. Liu, Y. Wu and H. Xu, Mechanism insights into Fe(III) reduction for enhanced aquatic contaminant degradation: The pivotal role of heterogeneous reductants, *Chem. Eng. J.*, 2023, **475**, 146495.
14 C. Gao, S. Chen, X. Quan, H. Yu and Y. Zhang, Enhanced Fenton-like catalysis by iron-based metal organic frameworks for degradation of organic pollutants, *J. Catal.*, 2017, **356**, 125–132.
15 L. Yu, B. Lu, Z. Liang, D. Wang, J. Liu, F. Wei, F. Wei and C. Liang, Enhancement of the heterogeneous photo-Fenton performance of GO/MIL-100(Fe)@Fe_3O_4 heterostructures for erythromycin degradation through accelerating Fe(II) generation, *RSC Adv.*, 2026, **16**, 5501.
16 J. Hang, X. Yi, C. Wang, H. Fu, P. Wang and Y. Zhao, Heterogeneous photo-Fenton degradation toward sulfonamide matrix over magnetic Fe_3S_4 derived from MIL-100(Fe), *J. Hazard. Mater.*, 2022, **424**, 127415.
17 L. Sun, X. Shen, H. Zhang and Y. Pang, Amino-functionalized iron-based MOFs for Rhodamine B degradation in heterogeneous photo-Fenton system, *J. Photoch. Photobio. A.*, 2024, **452**, 115544.
18 S. Huo and X. Yan, Metal–organic framework mil-100(Fe) for the adsorption of malachite green from aqueous solution, *J. Mater. Chem.*, 2012, **22**(15), 7449–7455.
19 H. Lv, H. Zhao, T. Cao, L. Qian, Y. Wang and G. Zhao, Efficient degradation of high concentration azo-dye wastewater by heterogeneous Fenton process with iron-based metal-organic framework, *J. Mol. Catal. A: Chem.*, 2015, **44**, 81–89.
20 X. Ma, B. Zhu, Z. Li, M. Wang, C. Miao, Y. Liu and S. Zhang, Environmentally friendly synthesis of quasi-MIL-100(Fe) with modulation defects for efficient photo-Fenton degradation of ciprofloxacin, *Sep. Purif. Technol.*, 2025, **363**, 131990.
21 W. He, Z. Li, S. Lv, M. Niu, W. Zhou, J. Li, R. Lu, H. Gao, C. Pan and S. Zhang, Facile synthesis of Fe_3O_4@MIL-100(Fe) towards enhancing photo-Fenton like degradation of levofloxacin via a synergistic effect between Fe_3O_4 and MIL-100(Fe), *Chem. Eng. J.*, 2021, **409**, 128274.
22 S. Rtimi, C. Pulgarin, R. Sanjines and J. Kiwi, Kinetics and mechanism for transparent polyethylene-TiO2 films mediated self-cleaning leading to MB dye discoloration under sunlight irradiation, *Appl. Catal., B*, 2015, **162**, 236–244.
23 C. Liers, E. Aranda, E. Strittmatter, K. Piontek, D. A. Plattner, H. Zorn, R. Ullrich and M. Hofrichter, Phenol oxidation by DyP-type peroxidases in comparison to fungal and plant peroxidases, *J. Mol. Catal. B-Enzym.*, 2014, **103**(5), 41–46.
24 H. Chen, S. Chen, X. Quan, Y. Zhao and H. Zhao, Sorption of perfluorooctane sulfonate (PFOS) on oil and oil-derived black carbon: influence of solution ph and [Ca2+], *Chemosphere*, 2009, **77**(10), 1406–1411.
25 H. Li, H. Yu, X. Quan, S. Chen and Y. Zhang, Uncovering the key role of Fermi level of electron mediator in Z-scheme photocatalyst by detecting charge transfer process of WO3-metal-gC3N4 (metal = Cu, Ag, Au), *ACS App. Mater. Interfaces*, 2016, **8**(3), 2111–2119.
26 F. Ke, L. Qiu, Y. Yuan, X. Jiang and J. Zhu, Fe3O4@mof core–shell magnetic microspheres with a designable metal–organic framework shell, *J. Mater. Chem.*, 2012, **22**(19), 9497–9500.
27 N. Chauhan, N. Sharma, S. Buhari, P. Das, S. Kumar and A. Chalana, Facile Synthesis of Copper Telluride Nanoparticles as a Robust Nanoenzymatic Catalyst for Intrinsic Peroxidase-Like Activity, *ChemistrySelect.*, 2024, **9**, e202304361.